Instabilities of nonisothermal nanocatalytic reactive flows in porous media

B. Dastvareh and J. Azaiez*
Department of Chemical and Petroleum Engineering, Schulich School of Engineering, University of Calgary, Calgary, AB, T2N 4V8, Canada

(Received 15 December 2018; published 13 March 2019)

Instabilities of reactive miscible flows in homogeneous porous media are investigated in the presence of nanocatalysts undergoing $A + B + n \rightarrow C + n$ reaction. The analysis is conducted under both isothermal and nonisothermal conditions resulting from the heat of reaction. Ignoring double diffusive effects of the different components, a new set of conditions is introduced to predict the instability of the isothermal case based on the species mobility ratios. Validated with nonlinear simulations, these conditions predict well the instability of the system and how the chemical product develops after the reaction. Examination of flows that account for the heat of reaction with no effect on the mobility ratios reveals that these conditions are no longer valid. This result is in contrast with nanocatalyst-free flows. In these systems the stability condition is unaffected by the heat of reactions that has neutral effects on mobility ratios. This difference is attributed to the nanocatalysts transport phenomena and in particular to thermophoretic effects arising from the temperature gradients in the flow. These effects are analyzed for both exothermic and endothermic chemical reactions.

DOI: 10.1103/PhysRevFluids.4.034003

I. INTRODUCTION

The interface of two approaching fluids in porous media becomes unstable at strong enough flow rates if a low viscous fluid displaces a high viscous one. The instabilities grow and develop fingerlike patterns that result in the mixing of the fluids. This phenomenon, called viscous fingering (VF), may be triggered or modified as a result of a chemical reaction and its control is important in several applications such as oil recovery [1,2], chromatographic separation [3], contaminant degradation [4], and polymerization fronts [5], to name a few. It has been reported that initially unstable systems become more unstable if the approaching fluids are reactive following autocatalytic reaction in the absence of chemical traveling wave [6,7]. Specifically, increasing both the mobility ratio of the fluids and Damköhler number (ratio of the diffusion to reaction time scales) intensifies this instability. An increase of the mixing zone between the fluids, enhancement of the tip splitting and the formation of droplets are other features observed in the presence of chemical reaction. However, the droplet formation and the finger propagation may be modified in the presence of chemical traveling wave [6,7]. Accounting for heat transfer effects through the temperature dependency of viscosity in autocatalytic reactive systems further increases the instability if the reaction is exothermic and mitigates it if it is endothermic. The Lewis number (ratio of the thermal to mass diffusivities), however, has an opposite effect such that it increases the instability in endothermic reactions while it suppresses it in exothermic ones [8]. Most existing studies on chemically driven viscous fingering have focused on a simple $A + B \rightarrow C$ reaction where the product C may have different viscosity than the displacing and displaced fluids A and B. In two separate experimental studies in a radial

*azaiez@ucalgary.ca

 ©2019 American Physical Society

Hele-Shaw cell [9,10], the dynamics of the flow in both reactive and non-reactive systems are investigated at similar unfavorable viscosity ratios. It was shown that the fingering patterns and the area occupied by the fingers are different in those systems, implying the effect of the reaction on the dynamics and the instability with unfavorable viscosity ratios. Later through some experiments in the same geometry it was observed that the initially stable system can even become unstable as a direct effect of $A + B \rightarrow C$ reaction [11]. However, although both the invading and displaced fluids had the same viscosity, the fingering patterns interestingly were different depending on which fluids are invading the other. Theoretical study of such initially isoviscous systems illustrated that the asymmetry in the finger patterns after the reaction emerges as a result of unequal concentrated reactants and/or the difference in their diffusivity [12]. A linear stability analysis (LSA) of systems involving a bimolecular $A + B \rightarrow C$ reaction was conducted by Hejazi *et al.* [13]. Since the rate of chemical production is time dependent, it was shown that the stability criteria change with the QSSA freezing time, t_0. However, asymptotically, it was found that initially unstable systems remain unstable after the reaction regardless of the viscosity of the products. In addition, depending on the viscosity of the chemical products, initially stable systems can become unstable as a result of the reaction. Nonlinear simulations (NLS) of such generic system were carried out for both moderate and infinite Damköhler numbers and the fingering patters were analyzed according the already classified stability conditions introduced by LSA [14,15]. As a result of the increase in use of nanocatalysts in different applications, particularly those for enhancing reaction rates in porous media [16–19], miscible VF instabilities of autocatalytic reactive isothermal systems have been investigated in the presence of dispersed nanocatalysts in the invading fluid [20,21]. It is reported that the increase in the viscosity of the invading fluid after the addition of nanocatalysts mitigates the instability of the reactive system. However, the presence of deposition which reduces both the reaction rate and the viscosity of the displacing fluid may lead to two opposing behaviors over time in terms of stability and the mixing rate. It is worth stressing that unless otherwise indicated, the above studies are conducted in a rectilinear geometry.

Although nanocatalysts have important effects on both the properties of the fluids and the reaction rate, there is still a lack of study on some aspects of the hydrodynamics instabilities in porous media. The objective of this study is to analyze the VF instabilities of nanocatalytic systems in the presence of $A + B + n \rightarrow C + n$ reaction which is more prone to create viscosity mismatch compared to the autocatalytic reaction. The analysis will first examine the case of isothermal flows and then focus on non-isothermal conditions that result from the heat of the reaction. This phase of the analysis is important as shall be seen later, the nanocatalysts are subject in particular to thermophoretic effects that have the potential to alter the dynamics of the flow.

II. PHYSICAL PROBLEM

A schematic view of the system is illustrated in Fig. 1 representing a homogeneous porous medium or equivalently a Hele-Shaw cell. The channel is initially occupied by a solution B with the initial mass fraction (or volume fraction in ideal solutions) of C_0 and the viscosity $\mu_{b_0} = \mu(0, C_0, 0, 0)$. Solution A with the same mass fraction of C_0 and the viscosity $\mu_{a_0} = \mu(C_0, 0, 0, 0)$ carrying nanocatalysts with initial mass fraction of C_{n_0} and the viscosity $\mu_{n_0} = \mu(0, 0, 0, C_{n_0})$ is injected into the channel at a velocity U. As soon as the solutions are in contact, the following reaction takes place:

$$A + B + n \rightarrow C + n. \tag{1}$$

The viscosity of the chemical product C at the mass fraction of C_0 is $\mu_{c_0} = \mu(0, 0, C_0, 0)$. Before the reaction takes place the system is at temperature of T_0, which may change after the reaction as a result of the change in the enthalpy, ΔH. $\Delta H < 0$ if the reaction is exothermic and $\Delta H > 0$ when it is endothermic. Finally, it is assumed that the fluids are incompressible and the nanocatalysts are in thermal equilibrium with the medium. Henceforth NP notation may refer to either nanocatalysts or nanoparticles.

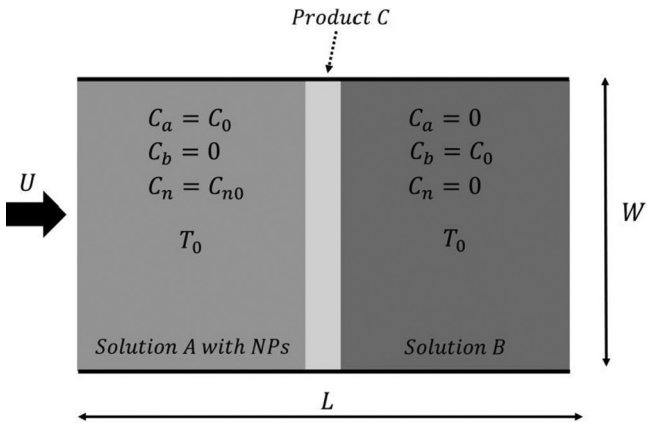

FIG. 1. Schematic view of the medium.

III. PROBLEM FORMULATION

The problem is governed by the following equations representing the conservation of mass, the conservation of momentum in the form of Darcy's law, transport of the components A, B, C, and NPs and finally the conservation of energy:

$$\vec{\nabla} \cdot \vec{V}_D = 0, \tag{2}$$

$$\vec{\nabla} P = -\frac{\mu}{K}\vec{V}_D, \tag{3}$$

$$\frac{\partial C_j}{\partial t} + \frac{1}{\phi}(\vec{V}_D \cdot \vec{\nabla} C_j) = D_j \nabla^2 C_j \pm r_R, \tag{4}$$

$$\frac{\partial C_n}{\partial t} + \frac{1}{\phi}(\vec{V}_D \cdot \vec{\nabla} C_n) = \vec{\nabla} \cdot \left(D_n \vec{\nabla} C_n + D_T \frac{\vec{\nabla} T}{T} \right) - k_{\text{dep}} C_n, \tag{5}$$

$$\frac{\partial T}{\partial t} + \frac{\lambda}{\phi}(\vec{V}_D \cdot \vec{\nabla} T) = \alpha \nabla^2 T - \frac{\phi \Delta H}{(\rho c_p)_m} r_R, \tag{6}$$

where $\vec{V}_D$ is Darcy's velocity, P the local pressure, μ the viscosity, and K the intrinsic medium permeability. In Eq. (4), $C_j = (C_a, C_b, C_c)$ is the mass/volume (in ideal solutions) fraction of the components, $D_j = (D_a, D_b, D_c)$ the corresponding diffusion coefficient, ϕ the porosity and r_R is the rate of reaction. D_j are assumed to be constant while the cross diffusion and Soret effects are ignored as they are an order of magnitude smaller than the principal diffusion effects. A first-order dependency on the concentration of the reactants and the NPs is adopted for the rate of reaction, where $r_R = k_R C_a C_b C_n$. Note that the linear dependency of the reaction rate on the nanocatalysts concentration has been reported in previous experimental studies [22–25]. Moreover, it is assumed that the heat of the reaction is small enough not to affect the dynamics through k_R which will be considered constant. D_n and D_T in Eq. (5) represent the Brownian and thermophoretic diffusion coefficients of NPs while k_{dep} is the deposition rate following the widely applied colloid filtration model [26]. Finally, $\lambda = \frac{\phi(\rho c_p)_{nf}}{(\rho c_p)_m}$ is the thermal lag coefficient [27] where the subscripts nf and m refer to the nanofuid and the medium, respectively, $\alpha = \frac{k_m}{(\rho c_p)_m}$ thermal diffusivity, ρc_p the volumetric heat capacity and k the thermal conductivity. Brownian and thermophoresis diffusion coefficients are in general not constant. In particular based on Einstein equation ($D_n = \frac{k_B T}{3\pi \mu_{bf} d_p}$) it is assumed that D_n varies linearly with temperature while following Piazza and Parola [28]

and Buongiorno [29], D_T in Eq. (5) is a linear function of C_n. Assuming $D_n = D_{n0}\frac{T}{T_0}$ and $D_T = D_{T0}\frac{C_n}{C_{n0}}$ [30] and incorporating constant K into the viscosity definition, the equations are then made dimensionless. Accordingly, the length, time, and pressure are scaled with $\frac{D_a\phi}{U}$, $\frac{D_a\phi^2}{U^2}$, $D_a\phi\mu_a$, viscosity with μ_a, velocity with U, C_j with C_0, and C_n with C_{n0}. Finally, the dimensionless temperature is defined as $\theta = \frac{T-T_0}{T_0 H_R}$, where $H_R = \frac{-\phi\Delta H C_0}{T_0(\rho c_p)_m} = \frac{\Delta T}{T_0}$. H_R, which is assumed to be small ($H_R \ll 1$) and does not lead to any fluid phase changes, represents the temperature changes as a result of the reaction. Finally, the equations are formulated in a reference frame moving with the velocity U. The equations are then in the following form:

$$\vec{\nabla}\cdot\vec{V} = 0, \tag{7}$$

$$\vec{\nabla}P = -\mu(\vec{V} + \vec{i}), \tag{8}$$

$$\frac{\partial C_j}{\partial t} + \vec{V}\cdot\vec{\nabla}C_j = \delta_j\nabla^2 C_j \pm \mathrm{Da}C_aC_bC_n, \tag{9}$$

$$\frac{\partial C_n}{\partial t} + \vec{V}\cdot\vec{\nabla}C_n = \delta_n\vec{\nabla}\cdot[(1+H_R\theta)\vec{\nabla}C_n] + \delta_T\vec{\nabla}\cdot[C_n\vec{\nabla}Ln(1+H_R\theta)] - \mathrm{Da}_{\mathrm{dep}}C_n, \tag{10}$$

$$\frac{\partial\theta}{\partial t} + (\lambda-1)\frac{\partial\theta}{\partial x} + \lambda(\vec{V}\cdot\vec{\nabla}\theta) = \mathrm{Le}\nabla^2\theta + \mathrm{sgn}(H_R)\mathrm{Da}C_aC_bC_n. \tag{11}$$

In these equations all the variables are dimensionless, where

$$\delta_j = \frac{D_j}{D_a}, \quad \delta_n = \frac{D_{n0}}{D_a}, \quad \delta_T = \frac{D_{T_0}}{D_aC_{n_0}}, \quad \mathrm{Le} = \frac{\alpha}{D_a}$$
$$\mathrm{Da}_{\mathrm{dep}} = \frac{k_{\mathrm{dep}}D_a\phi^2}{U^2}, \quad D_a = \frac{kD_a\phi^2C_0C_{n0}}{U^2}, \tag{12}$$

where δ_j, δ_n, δ_T are the solute, Brownian, and thermophoretic diffusivities, respectively, Da Damköhler number, Le Lewis number, and $\mathrm{Da}_{\mathrm{dep}}$ the dimensionless deposition rate. The positive sign in Eq. (9) is used for component C, while the negative sign is used for components A and B. Furthermore, $H_R > 0$ and accordingly $\mathrm{sgn}(H_R) = +1$ in the exothermic reaction, while $H_R < 0$ and $\mathrm{sgn}(H_R) = -1$ in the case of endothermic one. With the introduced scalings, the dimensions of the domain are $(-\frac{\mathrm{Pe}}{2}, \frac{\mathrm{Pe}}{2})$ in the x direction and $(0, \frac{\mathrm{Pe}}{A_s})$ in the y direction, where $\mathrm{Pe} = \frac{UL}{\phi D_a}$ is the Péclet number, and $A_s = \frac{L}{W}$ is the domain aspect ratio. In the moving reference, the concentrations of A, B, and NPs obey the zero flux condition at the x boundaries, while the velocity, C_c, and θ are zero. In addition, periodic boundary conditions are used in the y direction. The model is completed by adopting the following widely used exponential viscosity-concentration-temperature relationship [27,31]:

$$\mu = \exp(R_bC_b + R_cC_c + R_nC_n + R_\theta\theta), \tag{13}$$

where R_b, R_c, R_n, and R_θ are the mobility ratios defined as

$$R_b = \ln\left(\frac{\mu_{b_0}}{\mu_{a_0}}\right)_{T_0}, \quad R_c = \ln\left(\frac{\mu_{c_0}}{\mu_{a_0}}\right)_{T_0}, \quad R_n = \ln\left(\frac{\mu_{n_0}}{\mu_{a_0}}\right)_{T_0}, \quad R_\theta = \ln\left(\frac{\mu_{T_0(1+H_R)}}{\mu_{T_0}}\right). \tag{14}$$

$R_b > 0$, $R_c > 0$, and $R_n > 0$ indicate that the initial viscosities of the solutions made by components B, C, and NPs are greater than that of A, respectively. Furthermore, $R_\theta > 0$ in endothermic reactions, while $R_\theta < 0$ in exothermic ones.

IV. NUMERICAL METHODS

To solve the problem, the pressure is first eliminated from the equations by taking the curl of Darcy's law. Expressing the velocities in terms of the stream function and viscosity in terms of the concentrations and temperature, the equations are defined by vorticity (ω), stream function (ψ), concentrations (C_j, C_n), and temperature (θ). These equations are solved with the pseudospectral method [32]. In this method all the variable must be periodic at the boundaries. This is satisfied except for C_a, C_b, and C_n in the x direction. To solve this, the equations are formulated in terms of a base state $\bar{Y}(x,t)$ which satisfies the boundary conditions (BCs) and perturbations $Y'(x,y,t)$ that are periodic at the boundaries. The total variable $Y(x,y,t)$ is then determined by summation of the base state and perturbations. The base state equations for C_a, C_b, and C_n are as below, while $\bar{C}_c$, $\bar{\theta}$, $\bar{V}$ are zero:

$$\frac{\partial \bar{C}_a}{\partial t} = \frac{\partial^2 \bar{C}_a}{\partial x^2}, \tag{15}$$

$$\frac{\partial \bar{C}_b}{\partial t} = \delta_b \frac{\partial^2 \bar{C}_b}{\partial x^2}, \tag{16}$$

$$\frac{\partial \bar{C}_n}{\partial t} = \delta_n \frac{\partial^2 \bar{C}_n}{\partial x^2} - \mathrm{Da}_{\mathrm{dep}} \bar{C}_n. \tag{17}$$

Adopting $\bar{C}_a = H(-x)$, $\bar{C}_b = H(x)$, and $\bar{C}_n = C_{n0} H(-x)$ as the initial condition and zero flux boundary values, $\bar{C}_a(x,t) = \frac{1}{2} erfc(\frac{x}{2\sqrt{t}})$, $\bar{C}_b(x,t) = \frac{1}{2} erfc(-\frac{x}{2\sqrt{\delta_b t}})$, and $\bar{C}_n(x,t) = \frac{C_{n0}}{2} erfc(\frac{x}{2\sqrt{\delta_n t}})$. The perturbation equations are simply derived by subtracting the model equations from the base state equations:

$$\nabla^2 \psi' = -\omega', \tag{18}$$

$$\omega' = R_b N_b + R_c N_c + R_n N_n + R_\theta N_\theta, \tag{19}$$

$$\frac{\partial {C_j}'}{\partial t} = J_j + \delta_j \vec{\nabla} C_j' \pm \mathrm{Da}(\bar{C}_a + C_a')(\bar{C}_b + C_b')(\bar{C}_n + C_n'), \tag{20}$$

$$\frac{\partial {C_n}'}{\partial t} = J_n + \delta_n \vec{\nabla} \cdot [(1 + H_R \theta') \vec{\nabla} (\bar{C}_n + C_n')] + \delta_T \vec{\nabla} \cdot [(\bar{C}_n + C_n') \vec{\nabla} Ln(1 + H_R \theta')] - \delta_n \frac{\partial^2 \bar{C}_n}{\partial x^2} - \mathrm{Da}_{\mathrm{dep}} C_n', \tag{21}$$

$$\frac{\partial \theta'}{\partial t} = \lambda J_\theta + (1-\lambda) \frac{\partial \theta'}{\partial x} + \mathrm{Le} \nabla^2 \theta' + \mathrm{sgn}(H_R) \mathrm{Da}(\bar{C}_a + C_a')(\bar{C}_b + C_b')(\bar{C}_n + C_n'), \tag{22}$$

where

$$N_i = \frac{\partial \psi'}{\partial x} \left(\frac{\partial \bar{X}_i}{\partial x} + \frac{\partial {X_i}'}{\partial x} \right) + \left(1 + \frac{\partial \psi'}{\partial y} \right) \frac{\partial {X_i}'}{\partial y}, \tag{23}$$

$$J_i = \frac{\partial \psi'}{\partial x} \frac{\partial {X_i}'}{\partial y} - \frac{\partial \psi'}{\partial y} \left(\frac{\partial \bar{X}_i}{\partial x} + \frac{\partial {X_i}'}{\partial x} \right), \tag{24}$$

where $X_i = (C_j, C_n, \theta)$. The perturbation BCs are now periodic in both longitudinal and transverse directions. Furthermore, $\psi', \omega', C_c', \theta'$ are initially set to zero, while the random number distributions are allocated for C_a', C_b', and C_n'. More details are found in Ref. [32].

Finally, the numerical convergence has been checked and it was found that a grid of 256×128 is satisfactory for the range of considered parameters. The code has been validated for both nonreactive and reactive systems in the absence of NPs. First, setting $R_c = R_n = R_\theta = \mathrm{Da} = 0$ the

results are compared with available results for NP-free nonreactive systems. Subsequently, the finger configurations of a NP-free reactive system reported by Ref. [14] are compared with the results of the developed code by setting $R_n = R_\theta = 0$ and $C_n = 1$. In both cases the results were in good agreement with each other.

V. RESULTS AND DISCUSSION

The considered problem involves a large number of parameters. Therefore, to narrow them, the reference values of $\lambda = 1$, $\mathrm{Le} = 1$, $\delta_j = \delta_n = 1$, $\mathrm{Da} = 1$, $\mathrm{Da}_{\mathrm{dep}} = 0$, $A_s = 2$, and $\mathrm{Pe} = 1024$ are adopted unless otherwise indicated. Furthermore, to investigate the direct coupled effect of the presence of NPs and the heat of reaction, R_θ is set to be zero. This choice will be in particular valid when the heat of the reaction is localized at the interface where the reaction takes place, resulting in large temperature gradients and in turn strong thermophoretic effects while the overall changes in the temperature are not strong enough to induce noticeable changes in the fluids viscosities. Note that in NP-free reactive systems the presence of the heat of reaction has no effects on the instabilities if $R_\theta = 0$. Therefore, any changes in the dynamics of the system that may arise in the presence of NPs, will be interesting.

The analysis starts with NP-laden isothermal reactive systems. This analysis will allow to develop a classification of the reactive systems in terms of the mobility ratios of the different chemical species. The analysis is then expanded to analyze the effects of the heat of reaction in each classified NP-laden systems for both exothermic and endothermic reactions. This will be conducted qualitatively through the contours of C_c and quantitatively through the first moment of the transversely averaged product concentration as a representative of its center of mass and the cumulative concentration of the chemical products. The normalized first moment of the transversely averaged concentration of the products is defined as

$$x_m(t) = \frac{1}{\mathrm{Pe}} \int_{-\frac{\mathrm{Pe}}{2}}^{\frac{\mathrm{Pe}}{2}} x C_{c,\mathrm{av}}(x,t)\,dx, \tag{25}$$

where

$$C_{c,\mathrm{av}} = \frac{A_s}{\mathrm{Pe}} \int_0^{\frac{\mathrm{Pe}}{A_s}} C_c(x,y,t)\,dy. \tag{26}$$

Positive x_m indicates that the products are mostly developed downstream and vice versa. The normalized cumulated value of the chemical product is further defined as

$$(C_c)_t = \frac{A_s}{\mathrm{Pe}^2} \int_{-\frac{\mathrm{Pe}}{2}}^{\frac{\mathrm{Pe}}{2}} \int_0^{\frac{\mathrm{Pe}}{A_s}} C_c(x,y,t)\,dy\,dx. \tag{27}$$

It is expected that in the absence of NP deposition the value of $(C_c)_t$ increases monotonically as a result of the chemical reaction.

A. Isothermal reactions

In the absence of the heat of reaction ($H_R = 0$), $\theta = 0$ in the channel while the NP transport equation reduces to the simple form of $\frac{\partial C_n}{\partial t} = \delta_n \frac{\partial^2 C_n}{\partial x^2} - \mathrm{Da}_{\mathrm{dep}} C_n$. This equation is coupled with the other governing equations through the rate of reaction and viscosity which distinguishes it from the NP-free reactive systems. In the NP-free reactive systems involving a $A + B \rightarrow C$ reaction with constant diffusivities, it was already reported that if the system is unstable before the reaction ($R_b > 0$), it remains unstable after the reaction regardless of the value of R_c. However, in the case of an initially stable system ($R_b \leqslant 0$), the subsequent instability condition after the occurrence of the reaction depends on R_c. Specifically, the viscosity distribution is monotonically decreasing if $0 > \frac{R_c}{2} > R_b$ and the system is stable. However, the system is unstable if $0 < \frac{R_c}{2} < R_b$ where the viscosity

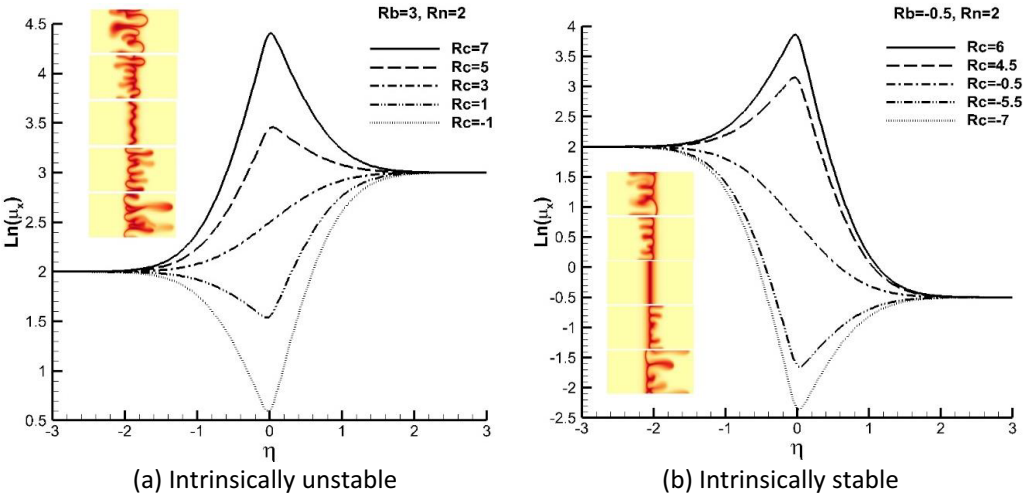

FIG. 2. One-dimensional Log-viscosity variation with respect to $\eta = \frac{x}{2\sqrt{t}}$ at asymptotically large times ($t \to \infty$) along with insets of corresponding contours of C_c derived from NLS. The contours are represented at $t = 1000$ for intrinsically unstable and $t = 1300$ for intrinsically stable systems.

is monotonically increasing or if $R_c(R_b - \frac{R_c}{2}) < 0$, where the viscosity distribution is nonmonotonic [13]. We will attempt here to extend these conclusions to NP-laden reactive $A + B + n \to C + n$ systems where NP has a catalytic role. Similarly, two systems are distinguished depending on whether the NP-laden systems are unstable or stable before the reaction. As reported in Ref. [33], in the absence of deposition, which is the focus of this study, the NP-laden nonreactive system is unstable if $R_b - R_n > 0$ and stable otherwise. Henceforth, we will refer to these two nonreactive NP-laden systems as intrinsically unstable and intrinsically stable, respectively. Adopting $R_b = 3$, $R_n = 2$ as an intrinsically unstable and $R_b = -0.5$, $R_n = 2$ as the intrinsically stable systems, the variations of the one-dimensional Log-viscosity with respect to the variable $\eta = \frac{x}{2\sqrt{t}}$ are presented at an asymptotic large time at Fig. 2. Insets of contours of C_c obtained from nonlinear simulations are included to illustrate the instability condition and show the finger configurations. The figure shows that, consistent with the results of the NP-free reactive systems, in the NP-laden reactive systems, intrinsically unstable systems remain unstable after the reaction as it generates either monotonically increasing or nonmonotonic viscosity distributions. However, initially stable systems may become unstable as a result of the nonmonotonicity in the viscosity distribution after the reaction. Furthermore, similar to the NP-free systems, in both cases the system with $R_c = R_b$ obeys the one-dimensional viscosity distribution in the form of error-function. This is the less unstable case after the reaction in the intrinsically unstable system according to the contours of C_c. However, as $|R_c - R_b|$ increases, both intrinsically stable and unstable systems are prone to more unstable situation as a result of the chemical reaction.

From Fig. 2 one may note that the viscosity variation may be different for $\eta > 0$ or $\eta < 0$ henceforth referred to as the leading zone and trailing zone, respectively [13]. Comparing the viscosity variations and the finger configurations, it is clear that monotonically increasing viscosities in any zone lead to more finger development in that region. Unlike the NP-free systems, the present viscosity variation is affected by R_n in addition to R_b and R_c in identical diffusivities.

To determine the exact condition for instability in each zone, the one-dimensional form of the governing equations in the direction of the flow is adopted to obtain the viscosity distribution μ_x. Accordingly, assuming $\delta_j = 1$, one concludes that $\frac{\partial(C_{ax}+C_{bx}+2C_{cx})}{\partial t} = \frac{\partial^2(C_{ax}+C_{bx}+2C_{cx})}{\partial x^2}$, and so with the defined boundary and initial conditions, $C_{ax} + C_{bx} + 2C_{cx} = 1$. Furthermore, it can be shown that $C_{bx} - C_{ax} = erf(\frac{x}{2\sqrt{t}})$. Taking advantage of these results and further assuming $\delta_n = 1$ to get rid of

double diffusivity effects and simply denoting $C_{n0}R_n$ by R_n, Eq. (28) is obtained in the absence of deposition. Note that in the presence of deposition, NPs are gradually removed from the system and the effect of R_n decreases with the passage of time. Furthermore, not only does the rate of deposition diminish the effect of R_n, but it also has a direct effect on the chemical product concentration and hence on R_c. So, the coupled effect of $\mathrm{Da}_{\mathrm{dep}}$ on the viscosity of the system and the production rate may have different effects on the dynamics of the flow. This, however, is not the focus of the present study and may be the subject of a separate investigation.

$$\frac{2}{\mu_x}\frac{\partial \mu_x}{\partial x} = (R_c - R_n)\left(-\frac{C_{ax}}{\partial x}\right) + (2R_b - R_c - R_n)\frac{C_{bx}}{\partial x}, \tag{28}$$

where if $\frac{\partial \mu_x}{\partial x} > 0$, then the viscosity distribution is monotonically increasing and the system is unstable and vice versa. Since $\frac{C_{bx}}{\partial x}$ and $(-\frac{C_{ax}}{\partial x})$ are positive, one can conclude that for $R_n \geqslant 0$, R_b has destabilizing and R_n has stabilizing effects, while the effect of R_c on the instability is nonmonotonic. As expected, this equation allows to distinguish two zones that develop as a result of the reaction; the leading zone with $R_L = 2R_b - R_c - R_n$ and the trailing one with $R_T = R_c - R_n$. Therefore, $R_L > 0$ and $R_T > 0$ indicate unstable zones and vice versa. It is concluded that the viscosity distribution will be monotonically increasing if $R_L > 0$ and $R_T > 0$ while it is monotonically decreasing if $R_L < 0$ and $R_T < 0$. However, if $R_L R_T < 0$ the viscosity distribution may be nonmonotonic where the flow is unstable. The special case of $R_b = R_c$ reduces the problem to that of a nonreactive NP-laden displacement while $R_c = R_n$ represents a neutrally stable trailing zone which implies no extremum in the viscosity distribution in this zone. However, the system with $R_b > R_n = R_c$ is more unstable than the intrinsically unstable system as the viscosity gradient now is confined in the smaller leading zone than the total channel. However, with $R_b < R_n = R_c$ the system is stable.

Assuming $R_b > R_n$ that represents an intrinsically unstable system, one can conclude that $2R_b - R_c - R_n > -(R_c - R_n)$. If $2R_b - R_c - R_n > 0$, then $R_c - R_n$ can be positive or negative while if $2R_b - R_c - R_n \leqslant 0$, then $R_c - R_n$ can only be positive. Accordingly, as long as $R_b > R_n$ at least one of the fronts is unstable, indicating that the intrinsically unstable system remains unstable after the reaction regardless of the value of R_c. Similarly, in the case $R_b \leqslant R_n$ corresponding to an intrinsically stable system, one has $2R_b - R_c - R_n \leqslant -(R_c - R_n)$. If $2R_b - R_c - R_n > 0$, then $R_c - R_n$ can only be negative, while if $2R_b - R_c - R_n \leqslant 0$, then $R_c - R_n$ can be either positive or negative. As a result, depending on the value of R_c, the intrinsically stable system will either remain stable or become unstable as a result of the reaction. These logical expressions further imply that depending on the particular values of R_b, R_c, and R_n where $R_c \neq R_b$ and R_n six different classes of systems can be identified in terms of their finger configuration. We will refer to them as Unstable (intrinsically unstable, both zones unstable after the reaction), IUD (intrinsically unstable, the leading zone unstable after the reaction where the products are mostly developed downstream), IUU (intrinsically unstable, the trailing zone unstable after the reaction where the products are mostly developed upstream), Stable (intrinsically stable, both zones stable after the reaction), ISD (intrinsically stable, the leading zone unstable after the reaction where the products are mostly developed downstream), and ISU (intrinsically stable, the trailing zone unstable after the reaction where the products are mostly developed upstream). Table I summarizes this classification with the representative mobility ratios for each case. The qualitative viscosity variation along the channel can be found in Fig. 2 for all the cases discussed.

Figure 3 presents the variation of x_m with time for two values of Da and shows where the products in each classified systems are developed. The representative systems for each class are $R_b = 3, R_n = 2, R_c = 2.5$ (Unstable), $R_b = 3, R_n = 5, R_c = 4$ (Stable), $R_b = 3, R_n = 2, R_c = 1$ (IUD), $R_b = 3, R_n = 2, R_c = 4$ (IUU), $R_b = -0.5, R_n = 2, R_c = -5$ (ISD), and $R_b = -0.5, R_n = 2, R_c = 5$ (ISU). Note that $x_m = 0$ in the Stable system as the system is diffusion dominant. However, as predicted, the products are more developed downstream ($x_m > 0$) in the IUD and ISD systems while they are more developed upstream ($x_m < 0$) in the IUU and ISU cases. Furthermore, $x_m > 0$ in the Unstable case as $R_L > R_T$. One may notice that the increase in x_m is monotonic in

TABLE I. Characteristics of classified isothermal systems.

System	Before the reaction	Unstable zone after the reaction
Unstable	Unstable ($R_b > R_n$)	Both ($2R_b - R_c - R_n > 0, R_c > R_n$)
IUD	Unstable ($R_b > R_n$)	Leading ($2R_b - R_c - R_n > 0, R_c < R_n$)
IUU	Unstable ($R_b > R_n$)	Trailing ($2R_b - R_c - R_n \leqslant 0, R_c > R_n$)
Stable	Stable ($R_b \leqslant R_n$)	None ($2R_b - R_c - R_n \leqslant 0, R_c < R_n$)
ISD	Stable ($R_b \leqslant R_n$)	Leading ($2R_b - R_c - R_n > 0, R_c < R_n$)
ISU	Stable ($R_b \leqslant R_n$)	Trailing ($2R_b - R_c - R_n \leqslant 0, R_c > R_n$)

both IUD and ISD systems as the direction of bulk flow is aligned with the fact that $R_L > 0$. In the ISU system, however, x_m is decreasing monotonically as the products experience strong resistance to flow downstream and so reverse to flow upstream instead. However, the behavior of x_m in the IUU and Unstable systems is nonmonotonic, indicating a competition between the bulk flow and the viscosity contrast effects.

NPs have a catalytic role in the present study and accordingly their transport has an impact on the total amount of chemical product. To analyze the effects of NPs on production and compare the trends with those of NP-free reactive systems, the variation in time of the total accumulated production is plotted in Fig. 4 for both NP-laden intrinsically unstable and stable systems by varying R_c. Again, $R_b = 3, R_n = 2$ and $R_b = -0.5, R_n = 2$ are selected as the mobility ratios of the NP-laden intrinsically unstable and stable systems, respectively. Note that in these figures as R_c is increased, the type of systems changes from IUD to Unstable and finally to IUU in the intrinsically unstable case, and from ISD to Stable and finally to ISU in the intrinsically stable systems. Figure 4 shows that in the Log-Log scale $(C_c)_t$ increases linearly in the diffusive regime similar to the NP-free reactive systems. Furthermore, in the IUD system increasing R_c leads to smaller chemical production until the system switches to an Unstable type ($R_c = 2.5$). The Unstable system has the lowest amount of the chemical product. Further increase in R_c changes the type of the system to IUU in which the amount of products starts to increase. Similarly, according to Fig. 4(b),

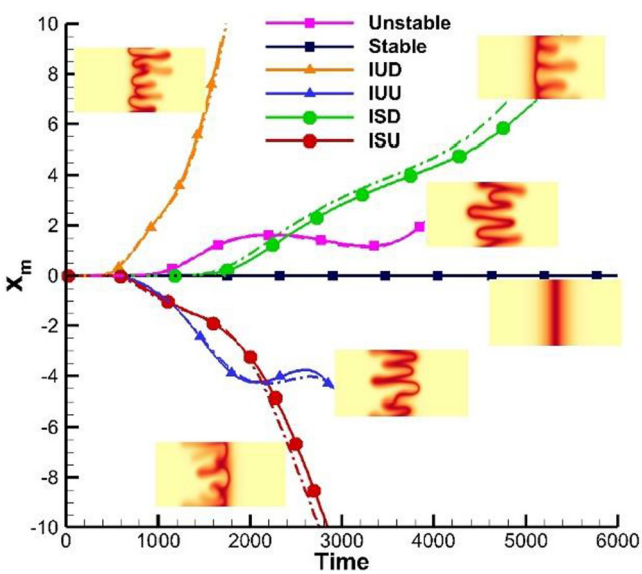

FIG. 3. Variation of the normalized first moment of the transversely averaged product concentration with the inset of contours of C_c. Dashed lines represent those systems with Da = 10.

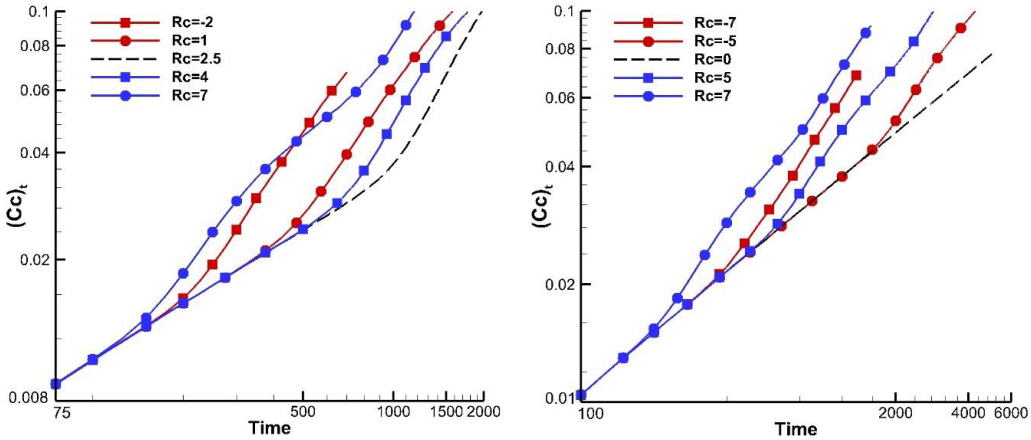

(a) Intrinsically unstable (b) Intrinsically stable

FIG. 4. The effect of R_c on the total amount of chemical products in the NP-laden isothermal reactive systems in the Log-Log scale.

as R_c increases the amount of chemical product in the ISD type decreases until the system becomes Stable ($R_c = -0.5$), where the amount of chemical product attains a minimum. Further increase of R_c changes the system to ISU type where the amount of chemical product is increased. These trends were observed with other choices of the values of the viscosity ratios and with a higher reaction rate of Da = 10. In the next section the present results will be extended to see the effect of the heat of reaction in the NP-laden catalytic systems.

B. Nonisothermal reactions

It is known that NP-free thermoviscous fingering instabilities both in the presence and absence of reaction develops as a result of the change in viscosity through R_θ [8,27,34]. Accordingly, if $R_\theta = 0$, then heat transfer does not affect the instability in the case of NP-free systems. However, since the temperature gradient resulting from the heat of reaction affects the transport of NPs, one may suspect that this effect may change the dynamics and the chemical products even if $R_\theta = 0$. To analyze this effect the results in the previous section are extended to include the heat of reaction but still for $R_\theta = 0$. Specifically, the effect of temperature driven NP transport which is represented by thermophoretic diffusivity δ_T is investigated in the already introduced representative Unstable, IUD, IUU, Stable, ISD and ISU systems while $H_R \neq 0$ for both exothermic and endothermic reactions.

1. Exothermic reactions

The objective here is to investigate the coupled effect of H_R and δ_T while the other heat transfer related properties are fixed. The analysis is first conducted for an exothermic reaction where the reference value of $H_R = 0.1$ is adopted. Figure 5 shows the variation of x_m for different thermophoretic diffusivities with insets of contours of the chemical product concentration C_c. The solid curves represent the reference systems at $\delta_T = 0$ and the dotted ones correspond to higher thermophoretic diffusivities. It is clear that for the set of adopted parameters, the variation of x_m in the absence of thermophoretic diffusivity is virtually identical to that in the isothermal system. However, at larger thermophoretic diffusivities the change in the variation of x_m is considerable. The figure shows that as δ_T increases, the transition time from the diffusion to the convective regime is reduced for systems with $x_m \geqslant 0$ and vice versa. Accordingly, at earlier times of convective regime thermophoresis leads to a systematic tendency for x_m to shift to more absolute values in systems with $x_m \geqslant 0$ and to less absolute values in systems with $x_m < 0$.

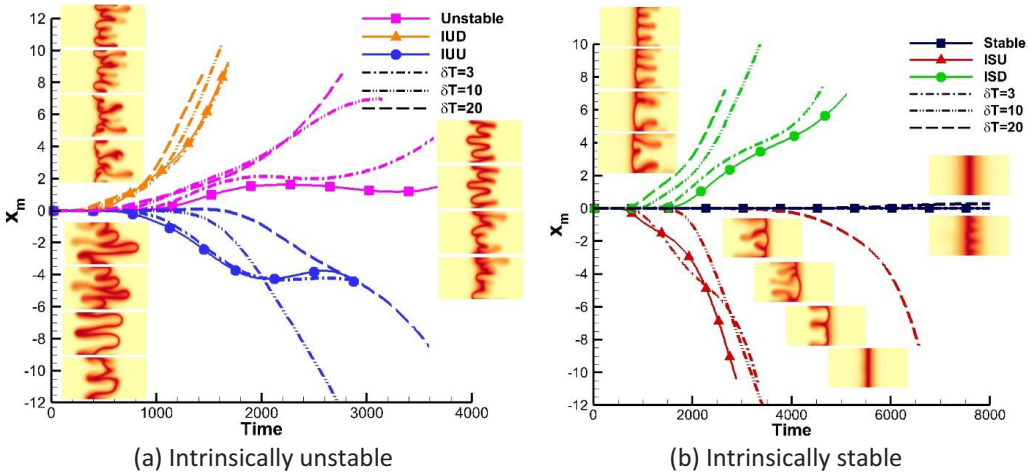

FIG. 5. The variation of x_m with time at different thermophoretic diffusivities in both intrinsically unstable and stable reference systems along with the inset of the contours of C_c. The contours are depicted at identical times in each systems. The solid lines represent the systems with $\delta_T = 0$.

At later time, $|x_m|$ still systematically increases with δ_T in IUD (except for a short interval) and ISD where only the leading zone is unstable. According to the finger configurations, this effect is attributed to more developed forward fingers or most importantly to the suppression of reverse fingering at higher δ_T. The same increasing trend is observed in the Stable case at high enough values of δ_T where the system becomes unstable with fingers developing downstream. Similar trends have been obtained in systems with larger Damköhler number, Da $= 10$.

In the IUU and ISU systems where only the trailing zone is unstable, a nonmonotonic trend is observed in the variation of x_m. However, at higher δ_T where thermophoretic effects are stronger, a general decreasing trend in the absolute value of x_m with increasing δ_T can be reported. According to finger configurations in both systems, backward fingers are suppressed at higher values of δ_T, which is the main reason for this trend. Further examination of the finger configurations reveals that for IUU and ISU systems, the products become confined in a narrow region as δ_T increases. In these systems the leading zone is locally stable and acts as a barrier to the upcoming flow. The upcoming flow as a result, returns and feeds the reverse fingers as the trailing front is unfavorable. However, with the suppression of reverse fingering at higher δ_T, the products have less possibility to move backward as well, and so get confined afterwards. The suppression of the forward fingers in addition to the backward fingers in IUU system is also attributed to this feature. Note that the backward finger suppression only delays the transport of the products upstream and the absolute value of x_m still increases at later times. Further analysis shows that this trend is virtually similar in higher reaction rates.

Finally, in the Unstable case the suppressed backward fingers now find the way to develop downstream as the leading zone is unstable. However, the forward fingers cannot accommodate all the upcoming flow. Accordingly, one may observe the confined products with few stretched fingers downstream at high δ_T. So, the general increasing trend for x_m with δ_T is observed and this trend is most noticeable at late times.

In summary, it is observed that the thermophoretic effects resulting from the heat of reaction alter both the finger configurations and the transport of the products. It can cause more developed or complex finger configurations in systems with unstable leading zone, leads to the suppression of backward product fingers, make the stable system unstable, and confine the chemical products in systems with leading stable zones (or even weak unstable zone). This affects the center of mass of the products as discussed above.

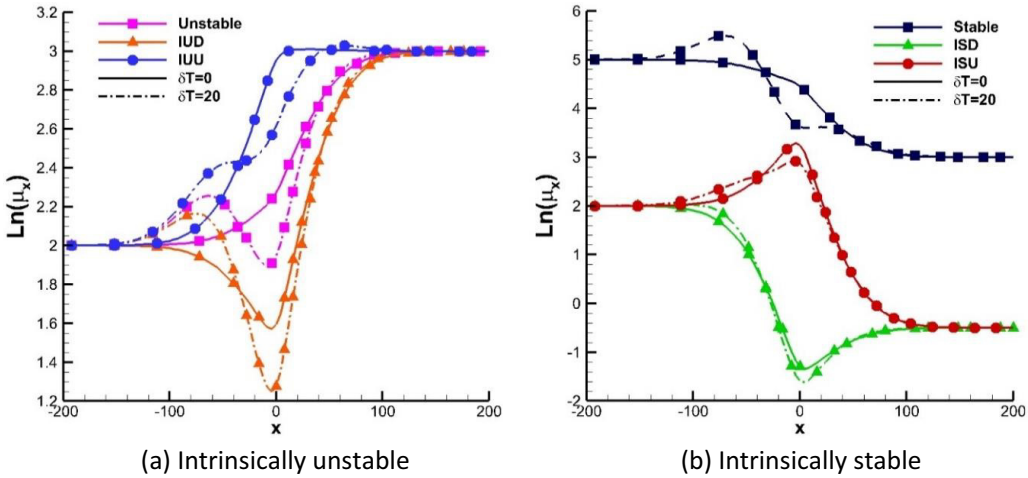

FIG. 6. The one-dimensional Log-viscosity variation in the reference systems in the presence ($\delta_T = 20$) and the absence of thermophoresis.

Figure 6 shows the corresponding one-dimensional viscosity distribution of the reference systems in the presence and absence of thermophoresis. Analyzing this figure elucidates the underlying reasons behind the changes in the variation of x_m shown in Fig. 5. The coupled effects of the viscosity increase at $x < 0$ and its decrease at the center cause the generation or intensification of locally stable regions in the trailing zone at $\delta = 20$ and result in a stronger resistance to the transport of the products upstream (in all systems except Stable). This important feature along with a sharper increase of the viscosity in systems with unfavorable leading zone (Unstable, IUD, ISD) at $x > 0$ and the fact that the monotonically decreasing viscosity distribution in the Stable system becomes nonmonotonic at $\delta_T = 20$, lead to the reported trends in the variations of x_m and the finger configuration.

One may wonder what triggers these changes in the flow behavior when the viscosities of the fluids are not changing with temperature variations ($R_\theta = 0$) and what is the role of heat of reaction? To attempt to answer this question, we examine the one-dimensional NP transport equation, Eq. (10):

$$\frac{\partial C_{nx}}{\partial t} = \delta_n(1 + H_R\theta_x)\frac{\partial^2 C_{nx}}{\partial x^2} + H_R\left(\delta_n + \frac{\delta_T}{1 + H_R\theta_x}\right)\frac{\partial \theta_x}{\partial x}\frac{\partial C_{nx}}{\partial x} + \delta_T\frac{\partial^2 Ln(1 + H_R\theta_x)}{\partial x^2}C_{nx}. \quad (29)$$

The first and second terms on the right-hand side represent diffusionlike and convectionlike contributions, respectively, while the third one is a source/sinklike term. This equation is solved along with the other coupled one-dimensional heat and concentration equations for different values of δ_T and H_R with the already-defined reference parameters. Note that since $u = 0$ in these 1D equations, the viscosity is decoupled from the equations and the choice of mobility ratios does not have any effects on the concentrations and temperature distributions. Accordingly with any arbitrary choice of mobility ratios, Fig. 7 shows the NP concentration distribution along the channel for different values of δ_T and H_R including the corresponding scaled variation of the convective term: $\text{Conv} = H_R(\delta_n + \frac{\delta_T}{1+H_R\theta_x})\frac{\partial\theta_x}{\partial x}$ and the source/sink term: $\text{Src} = \delta_T\frac{\partial^2 Ln(1+H_R\theta_x)}{\partial x^2}$. Note that $\text{Conv} = \text{Src} = 0$ at both ends of the domain and clearly everywhere in the case of the isothermal system. $\text{Conv} \leqslant 0$ with a local minimum for $x > 0$, while $\text{Conv} \geqslant 0$ with a local maximum for $x < 0$. Positive Conv leads to a negative thermophoretic velocity (NP velocity as a result of temperature gradient $V_t \propto -\frac{\partial\theta_x}{\partial x}$) and vice versa. However, Src experiences a local minimum with a negative value at the center and two positive local maxima at each side.

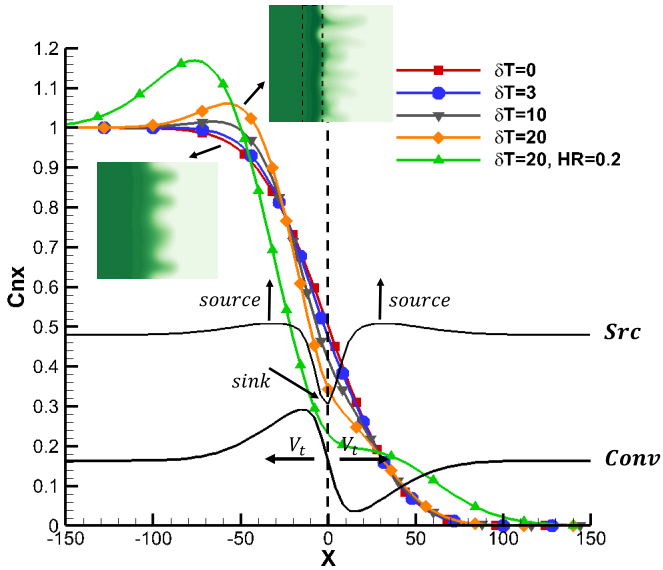

FIG. 7. The one-dimensional NP concentration variation at different δ_T with constant $H_R = 0.1$, and at two H_R with constant $\delta_T = 20$, including the scaled convective and source/sink terms variation. The representative inset of the contours of C_n derived from NLS are attached for $\delta_T = 0$ and $\delta_T = 20$.

The figure shows that by increasing δ_T and H_R, there is more accumulation of NPs at $x < 0$ and depletion at the center. Following a previous flow analysis [30], this behavior is a direct consequence of the temperature gradient driven convective transport of the NPs from the center to either sides of the channel. More specifically, the convected NPs from the center increase the local concentration of NPs at either side while NP concentration is decreased at the center, in the position of positive and negative Src, respectively. From the definition, both Conv and Src increase with increasing δ_T and H_R. This indicates that the two thermal-related terms, δ_T and H_R have synergic effects in the accumulation of NPs at either side of the channel and their depletion at the center. Accordingly as $R_n > 0$, a viscosity decrease at the center and its increases at $x < 0$ (considerably) and $x > 0$ (less pronounced) is expected if δ_T and H_R increase. This will affect the transport of the products, the variation of x_m, and the total chemical production. Note that there is not any accumulation or depletion if $\delta_T = 0$, although there is a convective velocity driven by the temperature gradient and Brownian diffusivity. This is because the convected NPs then diffuses according to the diffusive term $\delta_n(1 + H_R\theta_x)\frac{\partial^2 C_{nx}}{\partial x^2}$ in the absence of Src.

Now with the change in the transport of NPs discussed above, the question is how the amount of chemical products is changing in NP-laden reactive systems. We will examine next how the accumulated amount of chemical products is changing in the presence of thermophoretic effects with respect to the case in the absence of thermophoresis. Note that since with the set of parameters used, the total chemical production in the isothermal system is almost identical with that for $\delta_T = 0$, one can extend these results to compare it with the isothermal case as well.

Defining $(C_c)r_i = \frac{(C_c)_t(\delta_T=i)-(C_c)_t(\delta_T=0)}{(C_c)_t(\delta_T=0)}$, Fig. 8 shows the variation of $(C_c)r_i$ over time in the representative intrinsically unstable and stable systems, respectively. $(C_c)r_i > 0$ indicates that chemical production is larger than the case in the absence of thermophoresis and vice versa. According to Fig. 8(a), the presence of thermophoresis leads in a first stage of the flow to a larger production in both the IUD and Unstable systems. This trend is, however, subsequently reversed and $(C_c)r_i$ starts actually to decrease becoming later negative, implying that thermophoresis ultimately leads to smaller chemical production. Further analysis which for brevity is not shown here indicates that depending on the choice of parameters, the final value of $(C_c)r_i$ may not always be negative in

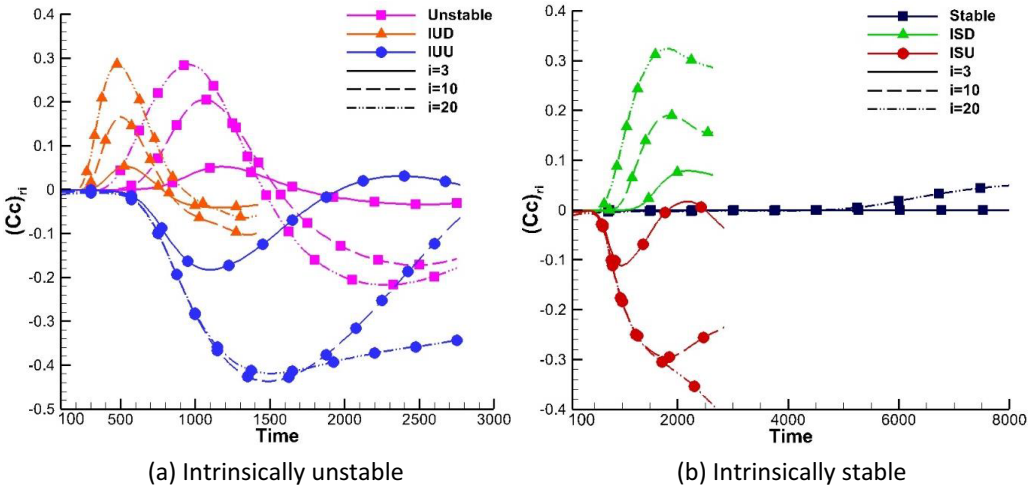

FIG. 8. Variation of $(C_c)_{r_i}$ in the representative systems at different thermophoretic diffusivities.

these systems. Opposite trends are found in the IUU system where the presence of thermophoresis results first in a decrease and then an increase of the relative chemical production. According to this figure, depending on the choice of parameters, the final relative production value in this case may actually lead to positive $(C_c)r_i$ indicating ultimate stronger chemical production than in the absence of thermophoretic effects. Note also that with increasing δ_T, chemical production is intensified in all the cases.

In contrast to the intrinsically unstable case, thermophoresis always leads to positive values of $(C_c)r_i$ in the ISD and negative ones in the ISU systems (except for a short interval when $\delta_T = 3$). This indicates that thermophoresis increases the chemical production in the ISD and decreases it in the ISU systems and this trend is intensified by increasing δ_T. Finally, interestingly large enough values of δ_T can lead to larger chemical production even in the representative Stable system as a direct effect of the developed instabilities. The analysis shows virtually identical trends with higher reaction rate of Da = 10 in all systems which for brevity are not shown here.

2. Endothermic reactions

In this section the previous analysis is extended to endothermic reactions. To start the analysis, let us examine the energy equation, Eq. (11). In this equation $\theta > 0$ and $\mathrm{sgn}(H_R) = +1$ in the exothermic reaction while $\mathrm{sgn}(H_R) = -1$ and $\theta < 0$ in the endothermic one. Accordingly, it is clear that with all parameters fixed, $\theta_{\mathrm{endo}}(x, y) = -\theta_{\mathrm{exo}}(x, y)$ if the distribution of C_a, C_b, and C_n are not changed by changing the type of reaction. In particular, by substituting $\theta(x, y) \to -\theta(x, y)$, the transport equation of the NPs and other components do not change if $H_R \to -H_R$. In addition, the viscosity distribution and the Darcy's law will not change as long as $R_\theta \to -R_\theta$ or $R_\theta = 0$. So, one can extend all the conclusion discussed about the exothermic reaction to the endothermic one if $H_R \to -H_R$. This conclusion was validated by NLS.

VI. CONCLUSION

The dynamics of nanoparticle-laden miscible reactive flows in homogeneous porous media are investigated when the nanoparticles (NPs) have catalytic effects and are dispersed in the invading fluid. The study is conducted in both isothermal and nonisothermal conditions considering the effect of heat of reaction. In the isothermal case, as long as $R_b > R_n$ the flow is unstable after the reaction regardless of the value of R_c, while the stability condition is dependent on R_c if

$R_b \leqslant R_n$. R_b, R_c, and R_n are the Log-viscosity ratios of the displaced fluid B, the chemical products C, and the nanofluid, respectively, to that of the displacing pure fluid A. Specifically, defining $R_T = R_c - R_n$ and $R_L = 2R_b - R_c - R_n$ as the effective viscosity ratios of the trailing and the leading zones, respectively, the viscosity distribution is monotonically increasing if $R_T > 0$ and $R_L > 0$, while it is monotonically decreasing when $R_T < 0$ and $R_L < 0$. However, its distribution may be nonmonotonic if $R_T R_L < 0$. The special case of $R_b = R_c$ reduces the problem to that of a nonreactive NP-laden displacement. The analysis showed that similar to nonreactive NP-laden systems, R_b and R_n has destabilizing and stabilizing effects, respectively. However, the effect of R_c on the instability is nonmonotonic. The dynamics of the products then can be categorized based on the condition of the system before the reaction (whether it is intrinsically stable or unstable) and the effective viscosity ratios of the trailing and leading zones after the reaction. This allowed to identify six cases as Unstable (intrinsically unstable, both zones unstable after the reaction), IUD (intrinsically unstable, the leading zone unstable after the reaction), IUU (intrinsically unstable, the trailing zone unstable after the reaction), Stable (intrinsically stable, both zones stable after the reaction), ISD (intrinsically stable, the leading zone unstable after the reaction), and ISU (intrinsically stable, the trailing zone unstable after the reaction).

The study reveals that in the presence of the heat of the chemical reaction that does not affect the mobility ratios, these stability conditions are no longer valid. This is in contrast with the NP-free systems where the dynamics of the flow in nonisothermal conditions are identical to those of isothermal systems if $R_\theta = 0$. Further analysis shows that this behavior is a result of thermophoretic effects that interfere with the transport of NPs at large enough values of H_R and δ_T. The synergic effects of the heat of reaction and thermophoretic diffusivity can lead to an accumulation of NPs at both zones and their depletion at the center in both exothermic and endothermic reactions. The NP accumulation is more pronounced at the trailing zone where they are more abundant. Then with positive R_n the viscosity distribution and accordingly the transport of the chemical products are changed. Specifically, the viscosity is locally increased and decreased in the regions with accumulated or depleted NPs, respectively. The new viscosity distribution results in more developed or complex finger configurations in systems with unstable leading zone, the suppression of the backward product fingers, making stable system unstable and confining the chemical products in systems with the leading stable (or weakly unstable) zones. Accordingly, the center of mass of the products is affected compared to the isothermal case.

Regarding to the chemical products, in intrinsically unstable systems, the heat of reaction-thermophoretic effects may have a nonmonotonic behavior compared to cases where thermophoretic effects are not accounted for. Specifically, defining $(C_c)r_i = \frac{(C_c)_t(\delta_T=i)-(C_c)_t(\delta_T=0)}{(C_c)_t(\delta_T=0)}$, in the IUD and Unstable systems $(C_c)r_i$ is first increasing with positive values in the passage of time, but later decreases and even becomes negative. However, an opposite trend is observed in the IUU systems. Depending on the choice of parameters the final value of $(C_c)r_i$ may not always be negative for the IUD and Unstable or positive in the IUU systems. Differently, the response of intrinsically stable systems to the heat of reaction-thermophoretic effects are monotonic. In other words, in the ISD and Stable systems $(C_c)r_i \geqslant 0$, while in the ISU system $(C_c)r_i \leqslant 0$.

ACKNOWLEDGMENTS

Support from the University of Calgary's Eyes High Scholarship program and the Natural Sciences and Engineering Research Council of Canada (NSERC) is acknowledged. The authors also acknowledge the use of computing resources of the West-Grid clusters.

[1] H. A. Nasr-El-Din, K. C. Khulbe, V. Hornof, and G. H. Neale, Effects of interfacial reaction on the radial displacement of oil by alkaline solutions, Rev. Inst. Fr. Pét. **45**, 231 (1990).

[2] V. Hornof and F. U. Baig, Influence of interfacial reaction and mobility ratio on the displacement of oil in a hele-shaw cell, Exp. Fluids **18**, 448 (1995).
[3] M. L. Dickson, T. T. Norton, and E. J. Fernandez, Chemical imaging of multicomponent viscous fingering in chromatography, AIChE J. **43**, 409 (1997).
[4] J. A. Cunningham and Z. J. Fadel, Contaminant degradation in physically and chemically heterogeneous aquifers, J. Contam. Hydrol. **94**, 293 (2007).
[5] J. A. Pojman, G. Gunn, C. Patterson, J. Owens, and C. Simmons, Frontal dispersion polymerization, J. Phys. Chem. B **102**, 3927 (1998).
[6] A. De Wit and G. M. Homsy, Viscous fingering in reaction-diffusion systems, J. Chem. Phys. **110**, 8663 (1999).
[7] A. De Wit and G. M. Homsy, Nonlinear interactions of chemical reactions and viscous fingering in porous media, Phys. Fluids **11**, 949 (1999).
[8] S. Swernath and S. Pushpavanam, Viscous fingering in a horizontal flow through a porous medium induced by chemical reactions under isothermal and adiabatic conditions, J. Chem. Phys. **127**, 204701 (2007).
[9] Y. Nagatsu, K. Matsuda, Y. Kato, and Y. Tada, Experimental study on miscible viscous fingering involving viscosity changes induced by variations in chemical species concentrations due to chemical reactions, J. Fluid Mech. **571**, 475 (2007).
[10] Y. Nagatsu, C. Iguchi, K. Matsuda, Y. Kato, and Y. Tada, Miscible viscous fingering involving viscosity changes of the displacing fluid by chemical reactions, Phys. Fluids **22**, 024101 (2010).
[11] T. Podgorski, M. C. Sostarecz, S. Zorman, and A. Belmonte, Fingering instabilities of a reactive micellar interface, Phys. Rev. E **76**, 016202 (2007).
[12] T. Gérard and A. De Wit, Miscible viscous fingering induced by a simple $a + b \rightarrow c$ chemical reaction, Phys. Rev. E **79**, 016308 (2009).
[13] S. H. Hejazi, P. M. J. Trevelyan, J. Azaiez, and A. De Wit, Viscous fingering of a miscible reactive $a + b \rightarrow c$ interface: A linear stability analysis, J. Fluid Mech. **652**, 501 (2010).
[14] S. H. Hejazi and J. Azaiez, Non-linear interactions of dynamic reactive interfaces in porous media, Chem. Eng. Sci. **65**, 938 (2010).
[15] Y. Nagatsu and A. De Wit, Viscous fingering of a miscible reactive $a + b \rightarrow c$ interface for an infinitely fast chemical reaction: Nonlinear simulations, Phys. Fluids **23**, 043103 (2011).
[16] R. Hashemi, N. N. Nassar, and P. Pereira Almao, Enhanced heavy oil recovery by *in situ* prepared ultradispersed multimetallic nanoparticles: A study of hot fluid flooding for athabasca bitumen recovery, Energy Fuels **27**, 2194 (2013).
[17] S. M. Shuwa, R. S. Al-Hajri, A. Mohsenzadeh, Y. M. Al-Waheibi, and B. Y. Jibril, Heavy crude oil recovery enhancement and *in-situ* upgrading during steam injection using Ni-Co-Mo dispersed catalyst, in *Proceedings of the SPE EOR Conference at Oil and Gas West Asia* (Society of Petroleum Engineers, 2016).
[18] J. B. Omajali, A. Hart, M. Walker, J. Wood, and L. E. Macaskie, *In-situ* catalytic upgrading of heavy oil using dispersed bionanoparticles supported on gram-positive and gram-negative bacteria, Appl. Catal., B **203**, 807 (2017).
[19] M. C. Chang, H. Y. Shu, W. P. Hsieh, and M. C. Wang, Using nanoscale zero-valent iron for the remediation of polycyclic aromatic hydrocarbons contaminated soil, J. Air Waste Manage. Assoc. **55**, 1200 (2005).
[20] K. Ghesmat, H. Hassanzadeh, J. Abedi, and Z. Chen, Frontal stability of reactive nanoparticle transport during *in situ* catalytic upgrading of heavy oil, Fuel **107**, 525 (2013).
[21] N. Sabet, S. M. Jafari Raad, H. Hassanzadeh, and J. Abedi, Dynamics of Miscible Nanocatalytic Reactive Flows in Porous Media, Phys. Rev. Appl. **10**, 054033 (2018).
[22] P. L. Freund and M. Spiro, Colloidal catalysis: The effect of sol size and concentration, J. Phys. Chem. **89**, 1074 (1985).
[23] H. N. McMurray, Particle size effects in electrocatalysis by uniform colloids of ruthenium dioxide hydrate, J. Phys. Chem. **98**, 9861 (1994).

[24] S. Carregal-Romero, J. Pérez-Juste, P. Hervés, L. M. Liz-Marzán, and P. Mulvaney, Colloidal gold-catalyzed reduction of ferrocyanate (iii) by borohydride ions: A model system for redox catalysis, Langmuir **26**, 1271 (2009).

[25] Y. Li, X. M. Hong, D. M. Collard, and M. A. El-Sayed, Suzuki cross-coupling reactions catalyzed by palladium nanoparticles in aqueous solution, Org. Lett. **2**, 2385 (2000).

[26] K. M. Yao, M. T. Habibian, and C. R. O'Melia, Water and waste water filtration: Concepts and applications, Environ. Sci. Technol. **5**, 1105 (1971).

[27] D. Pritchard, The instability of thermal and fluid fronts during radial injection in a porous medium, J. Fluid Mech. **508**, 133 (2004).

[28] R. Piazza and A. Parola, Thermophoresis in colloidal suspensions, J. Phys.: Condens. Matter **20**, 153102 (2008).

[29] J. Buongiorno, Convective transport in nanofluids, J. Heat Transfer **128**, 240 (2006).

[30] B. Dastvareh and J. Azaiez, Thermophoretic effects on instabilities of nanoflows in porous media, J. Fluid Mech. **857**, 173 (2018).

[31] C. T. Tan and G. M. Homsy, Stability of miscible displacements in porous media: Rectilinear flow, Phys. Fluids (1958–1988) **29**, 3549 (1986).

[32] M. N. Islam and J. Azaiez, Fully implicit finite difference pseudospectral method for simulating high mobility-ratio miscible displacements, Int. J. Numer. Methods Fluids **47**, 161 (2005).

[33] B. Dastvareh and J. Azaiez, Instabilities of nanofluid flow displacements in porous media, Phys. Fluids **29**, 044101 (2017).

[34] M. N. Islam and J. Azaiez, Miscible thermoviscous fingering instability in porous media. Part 1: Linear stability analysis, Transp. Porous Media **84**, 821 (2010).